PAPER

Check for updates

A bionic 3D-printed hydrogel microneedle of composite mesh for abdominal wall defect repair

Yangyang Liu,[a] Zhiqiang Zheng,[a] Yutong Liu,[b] Shurui Song,[a] Ruojing Li,[a] Lei Song,[a] Yeying Zhao,[a] Huajian Ren[*c] and Peige Wang [ID] [*a]

The use of mesh repair is a frequently employed technique in the clinical management of abdominal wall defects. However, for intraperitoneal onlay mesh (IPOM), the traditional mesh requires additional fixation methods, and these severely limit its application in the repair of abdominal wall defects. We drew inspiration from the adhesion properties of mussels for the present study, functionalized carboxymethyl cellulose (CMC) with dopamine (DA), and added polyvinyl alcohol (PVA) to the composite to further improve the wet adhesive ability of hydrogels. The CMC-DA/PVA hydrogel microneedles (MNs) were fabricated using an inverse molding technique, incorporating a 3D-printed thermoplastic polyurethane mesh to enhance mechanical strength. The tensile test and porcine skin adhesion test demonstrated that the hydrogel mesh exhibited satisfactory mechanical properties and adhesion in vitro, thus replacing the traditional fixed mesh in the treatment of rat full-thickness abdominal wall defects. The results of animal experiments revealed that the hydrogel mesh promoted the growth of new granulation tissue and inhibited inflammatory responses, thereby paving the way for a novel approach in treating full-thickness abdominal wall defects.

1. Introduction

Abdominal wall defects caused by trauma or congenital weakness of the abdominal wall affect millions of individuals worldwide. People are significantly affected by the disease, resulting in enormous social and economic pressures.[1,2] However, when the herniated abdominal viscera are incarcerated, ischemia and death of the involved organs can happen if not promptly treated.[3] Prompt surgical intervention is crucial for both abdominal trauma and congenital weakness of the abdominal wall in order to minimize the occurrence of organ damage and associated complications, such as infection, thereby reducing mortality.[4]

The principal approach to repairing abdominal wall defects is currently reinforcement with mesh on the basis of defect closure, and mesh bridging repair is only considered when closure of the defect cannot be achieved.[5,6] Polypropylene mesh (PP) has been widely used in abdominal wall surgery due to its favorable mechanical properties, biocompatibility, and chemical stability.[7] After it is transplanted into individuals, it causes both acute and chronic inflammatory reactions in surrounding

tissues, followed by fibrocyte proliferation and then fibrosis.[8–10] Scar tissue is formed that wraps the mesh so as to prevent the recurrence of the abdominal wall defects, but this is often accompanied by local discomfort and pain after surgery. Recurrent intestinal obstruction or even intestinal fistula occurs in severe cases, seriously affecting postoperative quality of life of patients.[9–11] Due to these reasons, the direct use of PP mesh for intraperitoneal onlay mesh (IPOM) was limited to a degree, as IPOM mainly relies on the suture, stapler, and other methods to affix the mesh. In addition, it requires higher technical expertise from surgeons. With the continuous progress in modern surgical technology and material science, abdominal wall surgery has increasingly developed in a more professional direction. The development of a self-adhering mesh of robust mechanical strength that is specifically designed for IPOM surgery is therefore essential for the management of abdominal wall defects.

Hydrogels are three-dimensional, hydrophilic polymer networks that are widely used in drug delivery, tissue engineering, and regenerative medicine,[12–14] and, intriguingly, mussels that live in the ocean show strong adhesion in moist environments due to their adhesive proteins,[15,16] which may also be used in surgical repair. Mussels generate adhesion through catechol structures that harbor two or three hydroxyl groups, and enhance adhesion through hydrogen bonding on the surface, $\pi-\pi$ stacking, metal chelation, and oxidative cross-linking of *o*-quinone groups.[16–18] It has been demonstrated that catechin-based adhesive hydrogels strongly adhere to any

aDepartment of Emergency Surgery, The Affiliated Hospital of Qingdao University, 16 Jiangsu Road, Qingdao 266000, P. R. China. E-mail: wpgzyz@163.com

bMedical Records Management Center, The Affiliated Hospital of Qingdao University, 16 Jiangsu Road, Qingdao 266000, P. R. China

cLab for Trauma and Surgical Infections, Department of Surgery, Jinling Hospital, Affiliated to Nanjing University, 305 East Zhongshan Road, Nanjing 210002, P. R. China. E-mail: rhj1288@163.com

surface, and carboxymethylcellulose (CMC) is a promising polysaccharide.[19–21] Because of its water solubility, low cost, and biodegradability, CMC is widely used in tissue engineering and drug delivery, and there is no need for a second surgery for CMC removal.[22,23] Based on these characteristics, we obtained a CMC-DA hydrogel with adhesive properties by an amide reaction between DA and CMC.

To further enhance the adhesive performance of the hydrogel mesh, the mesh can be securely anchored to the tissue *via* a microneedle (MN) technique in a minimally invasive manner.[24,25] By combining these components with thermoplastic polyurethane (TPU, a flexible and mechanically strong biocompatible material), mechanical strength is enhanced.[26] The printability of TPU also provides the possibility for personalized repair of abdominal wall defects in patients.

In this study, we developed a CMC-DA/PVA hydrogel by grafting DA to CMC for amidation and mixing them with different proportions of polyvinyl alcohol (PVA). We then poured the CMC-DA/PVA pre-gel solution into the negative mold followed by embedding a 3D-printed TPU mesh in the mold. The CMC-DA/PVA hydrogel MN mesh exhibits high

adhesion under wet conditions, and *in vitro* experiments have shown that the hydrogel mesh possesses good cytocompatibility. In addition, in a full-thickness abdominal wall defect model in rats, we verified that the hydrogel mesh promoted the growth of new granulation tissue and inhibited the expression of inflammatory factors. We hypothesize that this novel hydrogel composite mesh will show great potential in the treatment of full-thickness abdominal wall defects.

2. Results and discussion

2.1. Preparation and characterization of a CMC-DA/PVA hydrogel MN mesh

2.1.1. Characterization of CMC-DA by proton nuclear magnetic resonance (^{1}H NMR) and ultraviolet-visible (UV-vis) spectrophotometry. The synthesis process of the CMC-DA/PVA hydrogel MN mesh is shown in Fig. 1A and B. Under the addition of EDC- and NHS-activated carboxyl groups, the amino groups of DA and the carboxyl groups of the CMC backbone underwent an amidation reaction to form CMC-DA (Fig. 2A depicts the ^{1}H NMR spectra of CMC, DA, and CMC-DA). In contrast to CMC, a new signal at approximately 6.5 ppm (a) in
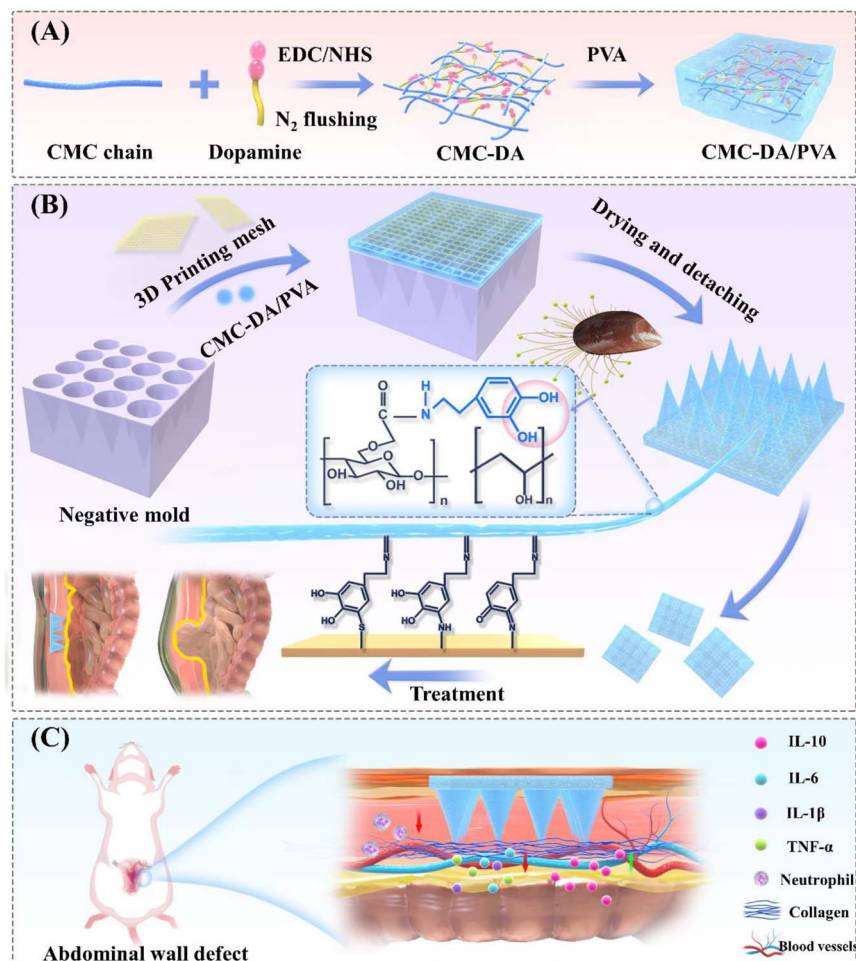

Fig. 1 Design diagram of CMC–DA/PVA hydrogel MN mesh. (A) Synthesis of CMC–DA/PVA hydrogel. (B) Preparation process of CMC–DA/PVA MN mesh. (C) Schematic diagram of multifunctional hydrogels for promoting abdominal wall defect repair.
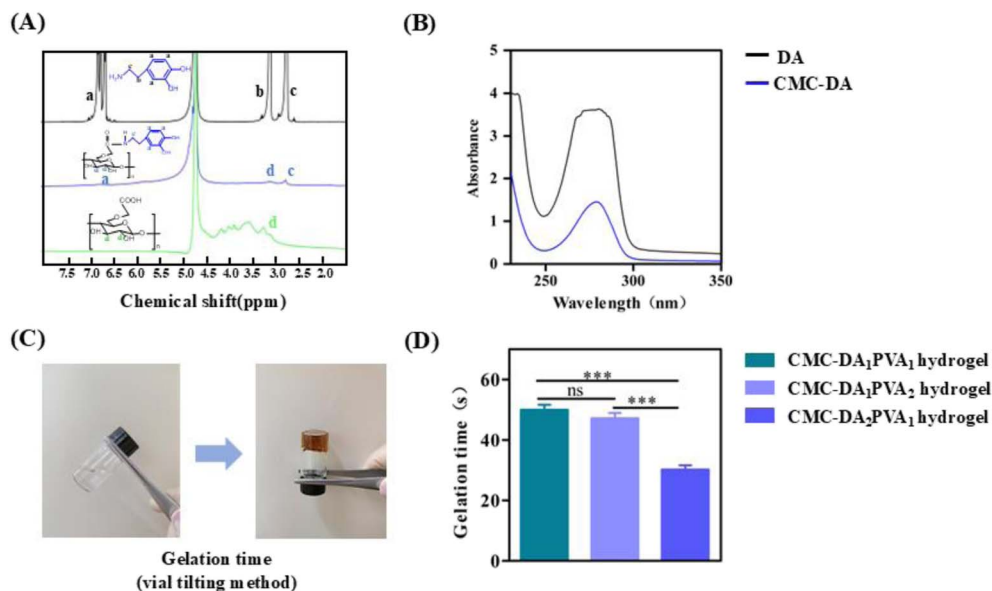
© 2025 The Author(s). Published by the Royal Society of Chemistry

Fig. 2 Characterization of CMC, DA, and CMC-DA hydrogels. (A) ^{1}H NMR spectra of the CMC, DA, and CMC-DA. (B) UV-vis spectra of DA and CMC-DA. (C) Photographs of formation of CMC-DA /PVA hydrogel by mixing with sodium periodate. (D) The gelation time of CMC-DA /PVA hydrogels with different compositions. The data are the mean ± SD ($n = 5$; ns = not significance compared with that of control group, ***$P <$ 0.001).
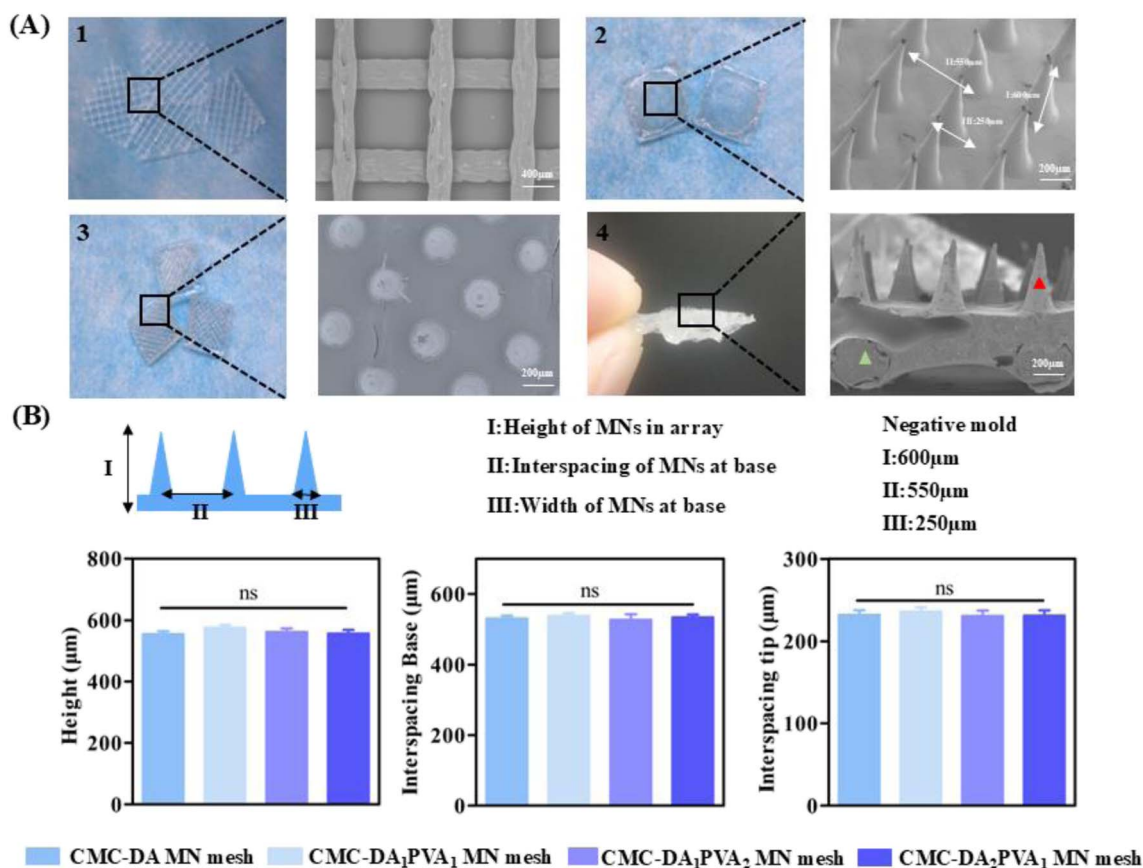

Fig. 3 Morphology of CMC-DA/PVA hydrogel MN mesh. (A) Scanning electron microscopy images of CMC-DA/PVA MN mesh. (B) Physical characteristics of MN arrays prepared from a series of CMC-DA/PVA hydrogel. The data are the mean ± SD ($n = 5$; ns = not significance compared with that of control group).
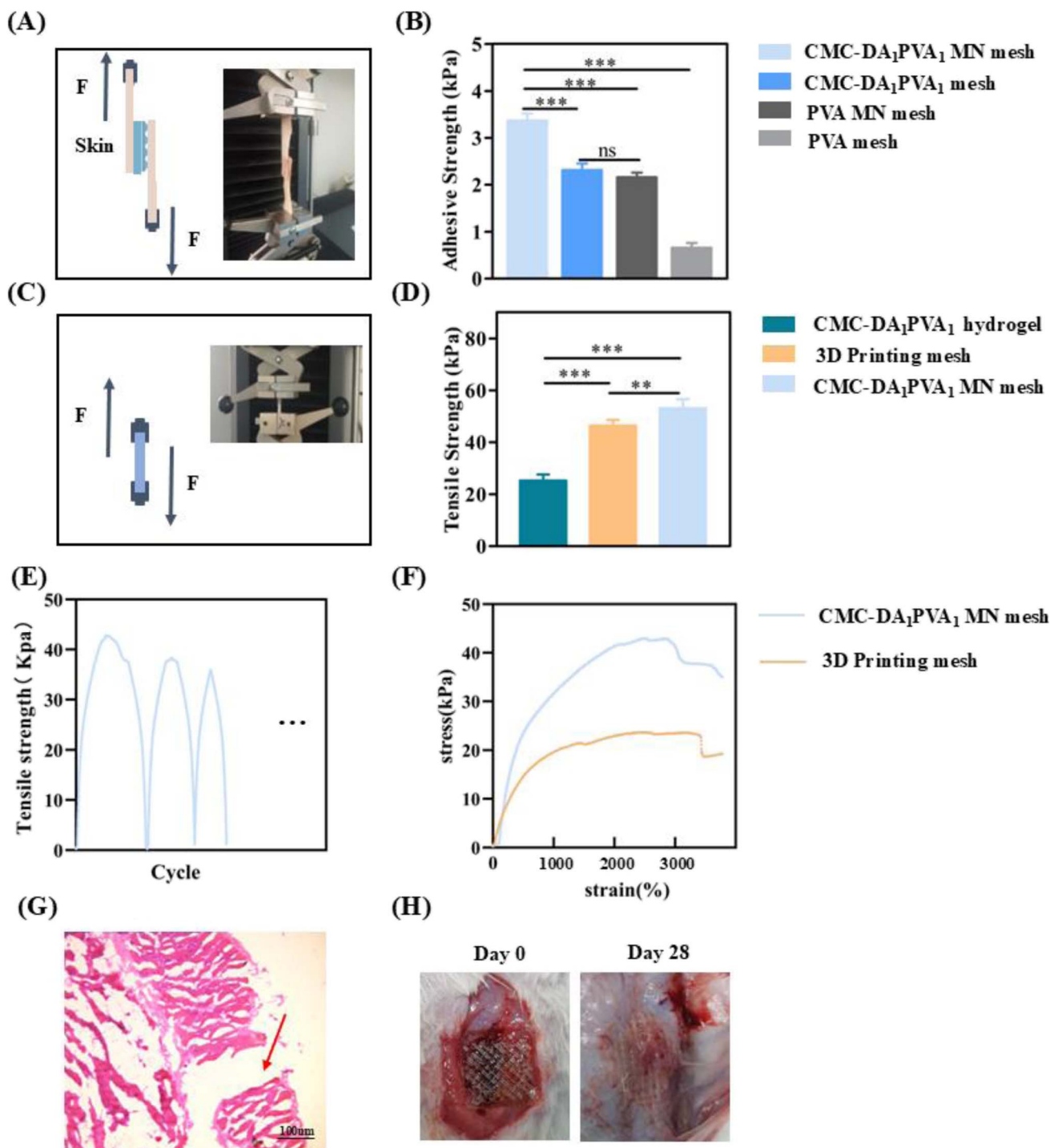
Fig. 4 Physical properties of the hydrogel. (A) Schematic diagram and photograph of the hydrogel adhesion test. (B) Adhesion strength of hydrogels with different components. The data are the mean $\pm$ SD ($n = 5$; ns = not significance compared with that of control group, ***$p <$ 0.001). (C) Schematic diagram and photograph of the hydrogel mechanical strength test; (D) mechanical strength of hydrogels with different components. The data are the mean $\pm$ SD ($n = 5$; **$p < 0.01$, ***$p < 0.001$). (E) The mechanical fatigue profile with CMC-DA$_1$/PVA$_1$ hydrogel MN mesh ($n = 5$). (F) Stress–strain curves of CMC-DA$_1$/PVA$_1$ hydrogel MN mesh and 3D printed mesh ($n = 5$). (G) HE staining of the muscle tissue of the abdominal wall where the CMC-DA$_1$/PVA$_1$ hydrogel MN mesh was inserted (arrows represent microneedle insertion into the tissue). (H) Gross morphological changes at different times after the CMC-DA$_1$/PVA$_1$ hydrogel MN mesh implantation in abdominal wall muscle tissue.

CMC-DA corresponded to a proton in the catechol aromatic ring, and a new signal at roughly 2.7 ppm (c) corresponded to a methylene proton between the catechol aromatic ring and the amino group,[27] implying that the conjugation reaction was successful (the UV-vis absorption spectra of DA and CMC-DA are shown in Fig. 2B). In contrast to DA, CMC exhibited an

emerging peak at 280 nm, indicating the successful conjugation of DA, with a substitution degree of 20.9%.

In order to determine the gel time for the CMC-DA/PVA hydrogel, CMC-DA and PVA of different components were matched and sodium periodate was added as an oxidant. Fig. 2C displays the sol–gel transition photographs of the CMC-DA polymer, with its color changing from transparent to brown instantly after introducing sodium periodate, which we attribute to the production of o-quinone groups via oxidation of catechol moieties (Fig. 2D shows the effect of CMC-DA and PVA concentrations on the gel time of CMC-DA/PVA hydrogels). Polymer gelation time varied from 55 s to 30 s with increasing CMC-DA concentration, which we attributed to an increased number of free radicals with the rise in CMC-DA concentration.

2.1.2. Morphology. The CMC-DA/PVA hydrogel MN meshes were characterized by scanning electron microscopy (SEM). Fig. 3A shows the structure of the CMC-DA/PVA hydrogel MN mesh, and Fig. 3A1 verifies the three-dimensional structure of the 3D-printed mesh. Fig. 3A2 shows that the surface of the hydrogel microneedles without a 3D-printed mesh was smooth and no collapse was observed. Fig. 3A3 shows the tip structure of CMC-DA/PVA hydrogel MN mesh, with the surface collapse visible due to the addition of a 3D-printed scaffold; however, this did not affect the microneedle structure (Fig. 3A4 shows a longitudinal section of the CMC-DA/PVA hydrogel MN mesh interspersed with the tip structure and 3D-printed mesh).

The design of the negative mold was as follows: a height of 600 μm, width of 250 μm at the base, and interspace of 550 μm. As shown in Fig. 3B, a series of CMC-DA/PVA MN meshes were successfully replicated from the negative mold. By comparing the height of the MNs in the array, interspace of MNs, and width of CMC-DA/PVA hydrogel MN meshes with different components, we found no significant differences among the groups. The formula for $CMC-DA_1/PVA_1$ was thus adopted for follow-up experiments with previously conserved materials.[28]

2.2. Physical properties of the $CMC-DA_1/PVA_1$ hydrogel MN mesh

2.2.1. Tissue adhesion. The adhesive strength of the $CMC-DA_1/PVA_1$ hydrogel MN mesh was measured by the lap shear test as shown in Fig. 4A. As depicted in Fig. 4B, of the four groups of hydrogel meshes, the adhesion of the $CMC-DA_1PVA_1$ MN mesh was the highest (3.368 kPa) relative to the $CMC-DA_1PVA_1$ mesh (2.311 kPa), PVA MN mesh (2.159 kPa), and PVA mesh (0.658 kPa); this further demonstrated that the tip structure improved the adhesion of the $CMC-DA_1/PVA_1$ hydrogel by enhancing the physical adhesion.

2.2.2. Mechanical strength. As shown in Fig. 4C, we conducted a mechanical strength test of the $CMC-DA_1/PVA_1$ hydrogel MN mesh using a universal mechanical machine. By comparing the mechanical strength of the $CMC-DA_1/PVA_1$ hydrogel, 3D-printed mesh, and $CMC-DA_1/PVA_1$ hydrogel MN mesh, we
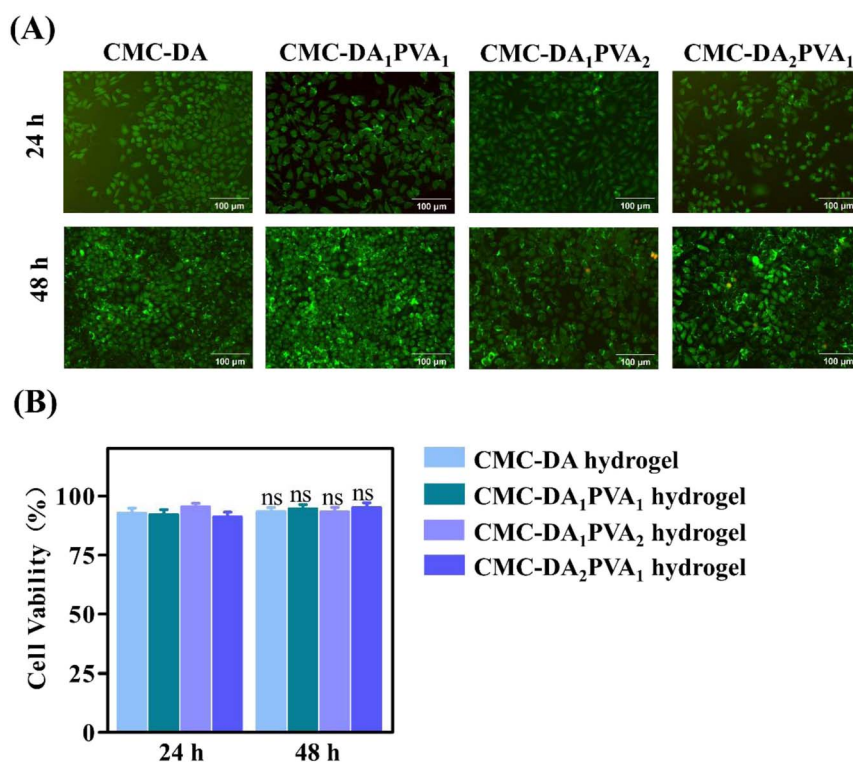

Fig. 5 Fibroblast evaluation of the *in vitro* cytocompatibility of CMC–DA/PVA hydrogel. (A) Fluorescence images of cytocompatibility of the hydrogels with different CMC–DA/PVA ratios. (B) CCK-8 test of hydrogels with different CMC–DA/PVA ratios. The data are the mean ± SD ($n = 5$; ns = not significance compared with that of control group).

ascertained that the CMC-DA$_1$/PVA$_1$ hydrogel MN mesh reflected superior mechanical strength (close to 60 kPa), and far exceeded normal intra-abdominal pressure. The tensile strength of the CMC-DA$_1$/PVA$_1$ hydrogel MN mesh was also significantly higher than normal intra-abdominal pressure (at 5 mmHg), and even higher than in grade IV abdominal-compartment syndrome (at 25 mmHg).[29] In addition, the CMC-DA$_1$/PVA$_1$ hydrogel MN mesh was more suitable in resisting the rapid increase in intra-abdominal pressure caused by coughing and sneezing (Fig. 4D). The mechanical fatigue profile was crucial for the CMC-DA$_1$/PVA$_1$ hydrogel MN mesh as it was to be used to treat abdominal wall defects. The results of mechanical-fatigue resistance testing on the CMC-DA$_1$/PVA$_1$ hydrogel MN mesh indicated that, although there was a visible decline in tensile performance after multiple tests, it still remained higher than level IV abdominal-compartment syndrome (Fig. 4E). Stress–strain curves of CMC-DA$_1$/PVA$_1$ hydrogel MN mesh and 3D printed mesh (Fig. 4F) show that CMC-DA$_1$/PVA$_1$ hydrogel MN hydrogel increases the tensile strength of CMC-DA$_1$/PVA$_1$ hydrogel MN mesh. H&E staining revealed that the CMC-DA$_1$/PVA$_1$ hydrogel MN mesh was inserted into the muscle tissue of the rat abdominal wall and penetrated the tissues so as to ensure good mesh anchoring (Fig. 4G). The CMC-DA$_1$/PVA$_1$ hydrogel MN mesh was also successfully integrated into the abdominal wall muscle tissue without displacement 28 days after implantation in the rats (Fig. 4H).

2.3. Cytocompatibility study

L929 cells play an essential role in a variety of tissue injuries and are often used to evaluate the biocompatibility of materials.[30] The cytocompatibility of the CMC-DA/PVA hydrogel was evaluated by the direct-contact method with fibroblasts, and Fig. 5A shows the fluorescent images of the stained cells, in which the dead cells were invisible. In addition, the CCK-8 assay in Fig. 5B confirmed that the cellular viability in all of the groups was higher than 90% at 24 h and 48 h. This implies favorable cytocompatibility of the components of the hydrogel and an absence of cytotoxic substances produced during the synthetic process.
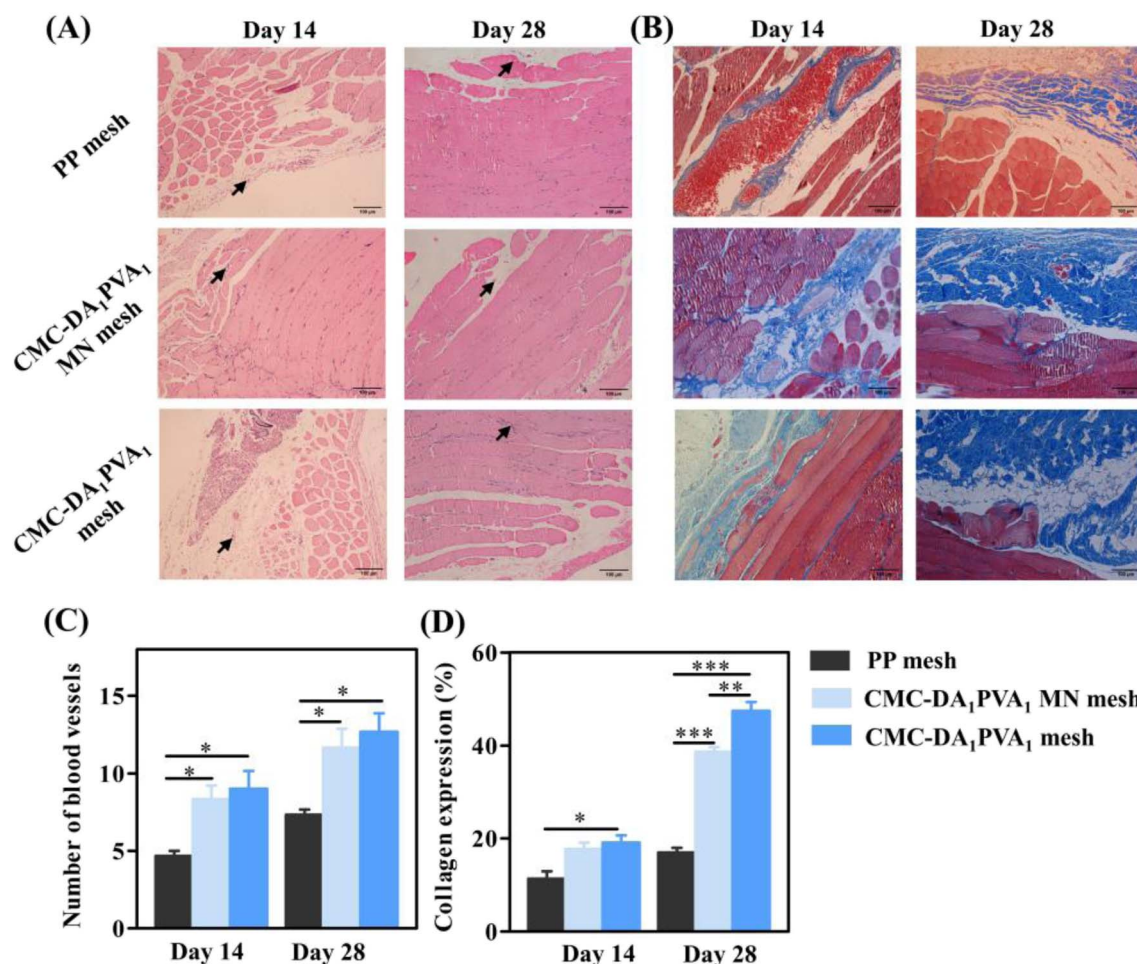

Fig. 6 Histological evaluation of three potential treatments for the protection of abdominal wall defect on rats. (A) HE staining of regenerative abdominal wall tissues (black arrows: new blood vessels). (B) Masson staining of regenerative abdominal wall tissues. (C) Quantitative analysis of the formation of new blood vasculature on the 14th, and 28th day. The data are the mean ± SD ($n = 5$; *$P < 0.05$). (D) Quantitative analysis of collagen formation. The data are the mean ± SD ($n = 5$; *$P < 0.01$, ***$P < 0.001$).
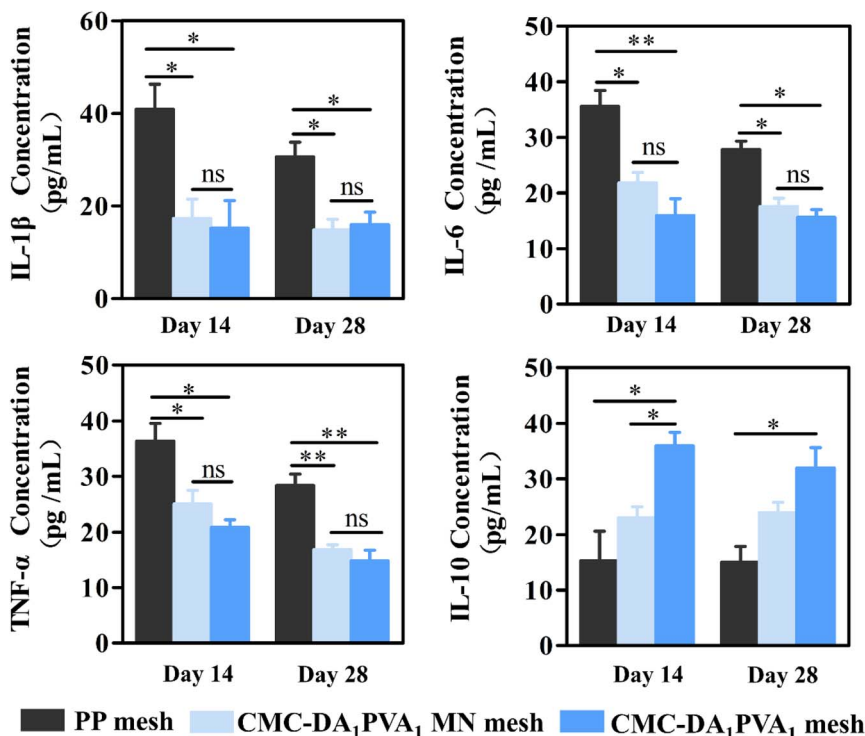
Fig. 7 Anti-inflammatory effect of CMC-DA /PVA hydrogel. Quantitative analysis of inflammatory factor expression in three groups. The data are the mean $\pm$ SD ($n = 5$; $*P < 0.05$, $**P < 0.01$, ns = not significance compared with that of control group).

2.4. Repair of an abdominal wall defect

To evaluate the healing ability of abdominal wall defects of the hydrogel *in vivo*, we conducted a repair experiment in a rat model (Fig. 1C). The wound-observation times of the CMC-DA$_1$/PVA$_1$ hydrogel MN mesh group, CMC-DA$_1$/PVA$_1$ hydrogel mesh group, and control group (PP mesh) were on days 14 and 28, and no animal deaths or recurrences of abdominal wall defects were noted. We observed the numbers of new blood vessels in the abdominal wall defects of rats in the three groups by optical microscopy (Fig. 6A). The rats were sacrificed on the 14th and 28th days after the operation, and compared with the control group, the number of new blood vessels in the CMC-DA$_1$/PVA$_1$ hydrogel MN mesh group and CMC-DA$_1$/PVA$_1$ hydrogel mesh group were increased (Fig. 6C). This indicated that the CMC-DA$_1$/PVA$_1$ hydrogel potentially facilitated tissue regeneration. However, the polyurethane did not degrade at 28 days, and no residue of polyurethane mesh was seen in the histopathological sections due to the separation of the polyurethane mesh from the tissue that occurred during specimen fixation.

As shown in Fig. 6B, Masson staining was used to show collagen deposition, and on the 14th day post-operatively and compared with the control group, the CMC-DA$_1$/PVA$_1$ hydrogel mesh group showed more obvious collagen production ($P < 0.05$, Fig. 6D). On the 28th day after the operation and compared with the controls, the CMC-DA$_1$/PVA$_1$ hydrogel MN

mesh group and CMC-DA$_1$/PVA$_1$ hydrogel mesh group showed more marked collagen production (Fig. 6D). These results revealed that the CMC-DA$_1$/PVA$_1$ hydrogel MN mesh promoted wound healing due to the synergistic biological effects of the CMC-DA hydrogel.

We quantified IL-6, IL-1β, TNF-α, and IL-10 in granulation tissue by ELISA to evaluate the inflammatory response during the repair of abdominal wall defects. The results in Fig. 7 show that IL-6, IL-1β, and TNF-α in the PP group were significantly higher than levels in the CMC-DA$_1$/PVA$_1$ hydrogel MN mesh group, while IL-10 in the PP group was significantly attenuated relative to levels in the CMC-DA$_1$/PVA$_1$ hydrogel MN mesh group, confirming the anti-inflammatory activity of the hydrogel. It is likely that the favorable biocompatibility of the hydrogel mesh reduced the stimulation to the damaged tissue, thus reducing the expression of inflammatory factors.

Non-toxic side-effects of the CMC-DA$_1$/PVA$_1$ hydrogel MN mesh on adjacent organs constitute a prerequisite in the repair of abdominal wall defects. Therefore, we evaluated the histopathological scores for liver and kidney, and our results showed that the histology of intra-abdominal organs (such as liver and kidney) of the hydrogel-coated animals remained normal (Fig. 8A and B), as there were no significant differences in histopathologic organ scores (Fig. 8C and D). This indicated that the CMC-DA$_1$/PVA$_1$ hydrogel MN mesh exerted no side effect on metabolic organs *in vivo*.
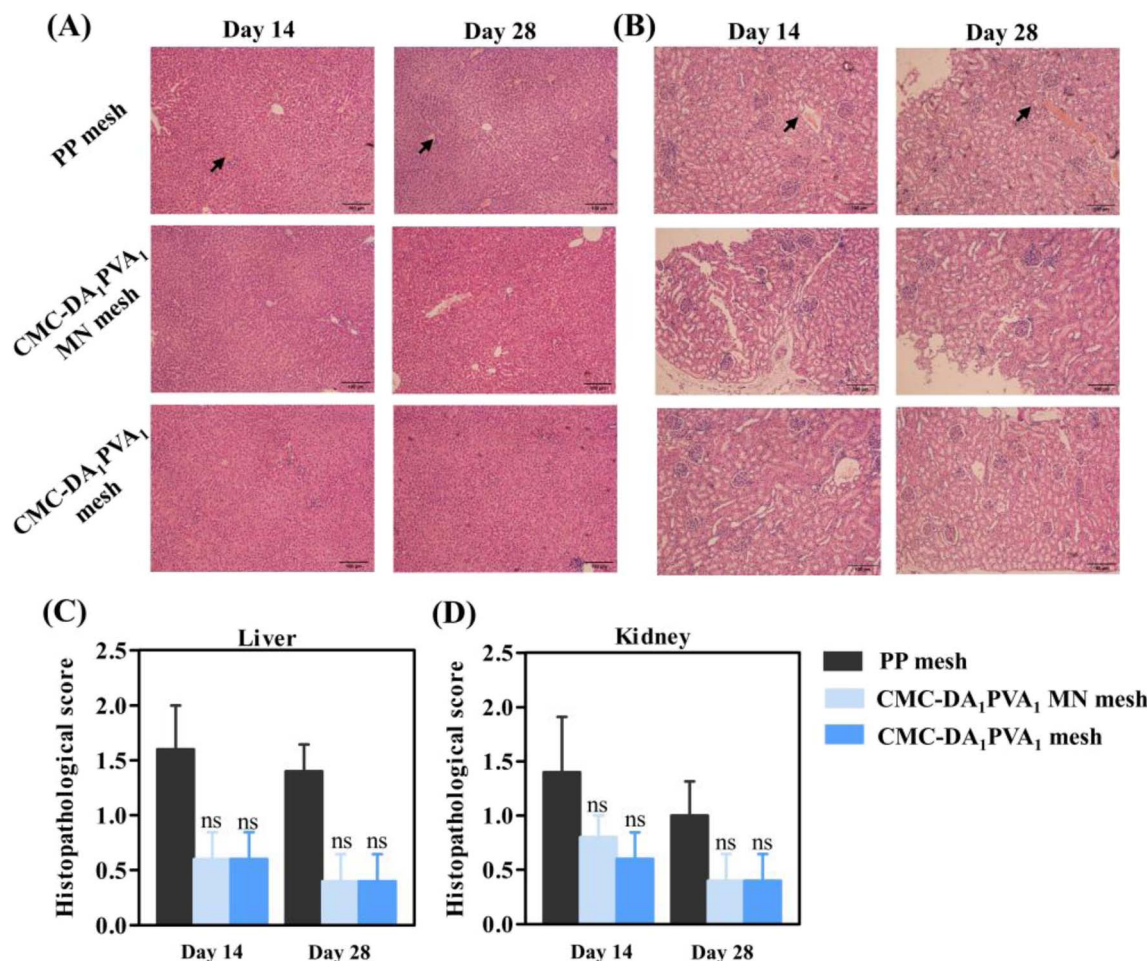
Fig. 8 Assessment of three potential treatments for organ toxicity on rats. (A and B) HE staining of liver and kidney on rats. (C and D) Pathological scores of major organs of rats from each group. The data are the mean ± SD ($n = 5$; ns = not significant compared with that of control group).

3. Conclusions

We herein prepared a hydrogel MN mesh with high adhesion and high mechanical strength by combining a CMC-DA/PVA hydrogel MN with a 3D-printed TPU mesh. The mesh exhibited both chemical adhesion (inspired by mussels) and physical adhesion that contributed to its MN structure. In this way, the CMC-DA/PVA hydrogel MN mesh was expected to replace the traditional clinical fixation mode, and thus shorten the operative time. The CMC-DA/PVA hydrogel MN mesh facilitated angiogenesis and collagen synthesis while suppressing inflammatory factor expression. Consequently, the mesh effectively enhanced abdominal wall strength and alleviated patient discomfort. Therefore, the CMC-DA/PVA hydrogel MN mesh demonstrated significant potential in repairing full-thickness abdominal wall defects.

4. Materials and methods

4.1. Materials, cell lines, and animals

We purchased carboxymethyl cellulose (CMC, 250 kDa), dopamine (DA, 98%), N-hydroxysuccinimide (NHS), and 1-(3-

dimethylaminopropyl)-3-ethylcarbondiimide hydrochloride (EDC) from Alighting Industries (China). Polyvinyl alcohol (PVA) and negative mold were from Suzhou Yongqinquan Intelligent Equipment Co., Ltd.; and PP mesh was provided by B. Braun Medical International Trading Co., Ltd. Cell medium was prepared using Dulbecco's Minimum Essential medium (DMEM, Gibco, US) with 10% fetal bovine serum and 1% penicillin–streptomycin. A CCK-8 Cell Proliferation Kit and Live/Dead Stain Detection Kit were purchased from KeyGen Biotech Co., Ltd. We bought the L929 cell line from Procell Life Science & Technology Co., Ltd. (China). Adult male Sprague-Dawley rats (220 ± 30 g) were used for all of the animal experiments, and animals were housed under a 12 h light–dark cycle at a constant temperature (23 ± 1 °C) and relative humidity ($50 \pm 5\%$). Animal experimental protocols were approved by the Animal Investigation Ethics Committee of the Affiliated Hospital of Qingdao University (license number AHQU20210702).

4.2. Fabrication of the hydrogel

4.2.1. Synthesis of the CMC-DA hydrogel. Per a previous method,[27] CMC-DA polymer was synthesized by the coupling

reaction between CMC and DA under the catalysis of EDC/NHS, and the solution was stirred overnight. First, CMC (0.25 g, 1.03 mmol carboxyl group) was dissolved in 50 mL of PBS buffer solution (pH = 5) and stirred overnight. After that, 0.158 g of DA and 0.119 g of NHS were added to the CMC solution and stirred for 30 min, and 0.197 g of EDC was subsequently added to the NHS in an equimolar ratio. The reaction was carried out at 30 °C for 24 h. Since DA is easily oxidized, the entire reaction process was conducted in a nitrogen environment protected from light. The products were subsequently purified with PBS buffer for one day and with deionized water for two days, with three changes per day. During dialysis, the dialysate was measured with UV-vis spectrophotometry (SHIMADZU UV-2550) to ensure that free DA and other catalysts were completely removed. The final product was ultimately lyophilized and stored.

4.2.2. Preparation of the CMC-DA/PVA hydrogel MN mesh.
CMC-DA (0.1 g) was dissolved in 10 mL of double-distilled water and mixed with 10% PVA. CMC-DA (1%) and 10% PVA were then mixed according to mass concentration ratios of 1 : 1, 1 : 2, and 2 : 1. The 3D-printed TPU mesh was cut into a 1.5 × 1.5 cm square and placed in the negative mold, and the CMC-DA/PVA pre-gel solution was injected into the negative mold (height of MNs in the array, 600 μm; interspacing of MNs at the base, 550 μm; and width of the MNs at the base, 250 μm), followed by defoaming under negative pressure and drying in an incubator at 30–35 °C for 5–6 h. Subsequently, another appropriate amount of CMC-DA/PVA pre-gel solution was added and dried for 5–6 h before releasing the mold to obtain the CMC-DA$_1$/PVA$_1$ hydrogel MN mesh, CMC-DA$_1$/PVA$_2$ hydrogel MN mesh, and CMC-DA$_2$/PVA$_1$ hydrogel MN mesh respectively.

4.3. Characterization of materials

4.3.1. Characterization of CMC-DA.
With respect to confirmation of CMC-DA conjugation, the NMR spectra of CMC, DA, and CMC-DA dissolved in deuterated solvents were characterized by ^{1}H NMR (Bruker, Germany). The conjugation efficiency of the CMC-DA side-chain was determined using a UV-vis spectrophotometer (PerkinElmer, USA) by measuring the absorbance at 280 nm of the CMC-DA solution with known concentrations and then calculating from a calibration curve of dopamine.

4.3.2. Characterization of the CMC-DA/PVA hydrogel MN mesh.
We characterized the morphology of the CMC-DA/PVA hydrogel MN using scanning electron microscopy (SEM, Hitachi, Japan) at an accelerating voltage of 20 kV. The CMC-DA/PVA hydrogel MN mesh was coated with a thin layer of gold prior to the observation.

4.4. Tissue adhesion

To quantify the adhesive properties of the CMC-DA$_1$/PVA$_1$ hydrogel MN mesh, we measured its adhesive strength by lap shear test.[31] To mimic the actual nature of human tissue, wet pig skin was adopted as a matrix material because it is the closest structurally and functionally to human skin. As a typical model for adhesive strength tests, pigskin matrix in a 2 mm thickness was cut into strips at a width of 1.5 cm and a length of

3 cm. We fix the smooth surface of the microneedle to the skin by means of sutures. A 10% sodium periodate solution was evenly coated on the surface of the CMC-DA$_1$/PVA$_1$ hydrogel MN mesh, and the MN mesh was placed between two layers of pig skin. The layers were then quickly stacked and pressed for 2 h at 37 °C with 100 g weights. A universal testing machine equipped with a 3000 N loading unit was used to test the adhesive strength at a rate of 5 mm min^{-1} at room temperature. Each measurement was repeated at least five times. The adhesive strength was calculated as the maximal load divided by the overlapping contact area (1.5 × 1.5 cm) according to the following formula:

$$\text{Adhesive strength} = \frac{F(\text{tensile force})}{S(\text{contacting area})}$$

4.5. Determination of mechanical strength

The CMC-DA$_1$/PVA$_1$ hydrogel MN mesh, CMC-DA$_1$/PVA$_1$ hydrogel, and 3D-printed TPU mesh were placed in a universal mechanical machine (Hengyi, HY-0580, China), and tensile strength was determined at a strain rate of 5 mm min^{-1} at room temperature.

4.6. Cytocompatibility study

The cytotoxicity of the CMC-DA/PVA hydrogel was evaluated by a direct-contact method using L929 fibroblasts. One hundred microliters of CMC-DA/PVA hydrogel was added to each well of a 96-well cell culture plate and rinsed with PBS solution. Cells were seeded on 200 μL of medium at a density of 5.0×10^4 cells per well and incubated for two days at 37 °C in a 5% CO$_2$ incubator. Cellular viability was measured using a CCK-8 assay, and absorbance of the solution was measured using a Multiskan FC Microplate Reader (Thermo, US) at 490 nm.

We calculated cellular viability using the following equation:

$$\text{Cell viability} = \frac{A_t - A_0}{A_c - A_0} \times 100\%,$$

where A_t, A_0, and A_c represented the absorbance of the sample groups, control groups, and blank groups, respectively; the tests were conducted in triplicate. After the same cell treatment, cells were stained with acridine orange and ethidium bromide (AO/EB) double-fluorescent dyes and observed with an Olympus LX70-140 inverted fluorescence microscope.

4.7. Assessment of full-thickness abdominal wall defect *in vivo*

Twenty-four male Sprague-Dawley rats (180–250 g) were fasted overnight and then anesthetized *via* intraperitoneal injection of 10% chloral hydrate at 0.3 mL 100 g^{-1}. Under an aseptic surgical technique, 1.5 × 1.5 cm lateral wall defects of the external oblique muscle, internal oblique muscle, and transverse abdominal muscle were established, while the skin and peritoneum of the rats were conserved. The control group harbored a PP mesh affixed to the defect's edge, with suturing performed using non-absorbable 4–0 wire. In the experimental

group, the CMC-DA$_1$/PVA$_1$ hydrogel MN mesh was uniformly coated with 10% sodium periodate as an oxidant, and the abdominal wall defect was repaired by touching the peritoneum with the microneedle surface and the smooth surface of the microneedle mesh. The microneedle surface and smooth surface were respectively defined as the CMC-DA$_1$/PVA$_1$ hydrogel MN mesh and the CMC-DA$_1$/PVA$_1$ hydrogel mesh.

We photographed the rat abdominal wall defects on days 14 and 28. The rats were anesthetized and new granulation tissue of the abdominal wall was collected for subsequent experiments. Each granulation tissue sample was cut into two parts: one part was immersed in 10% neutral formaldehyde for H & E staining and Masson tri-chrome staining; and the other portion was ground for ELISA analysis. Finally, the principal tissues—including liver and kidney—were harvested for further histological examination. After H & E staining, the sections were analyzed by professional pathologists.

Our pathological evaluation criteria were as follows. Edema, structural changes, and inflammatory cell infiltration of various organ lesions—from light to heavy—were divided into four degrees, corresponding to 0–4 points: *i.e.*, 0, no or very slight damage; 1, mild injury; 2, moderate injury; 3, severe injury; and 4, very severe damage.[32] The final score was the summation of the scores of each sample. All of the animal care and experimental protocols were performed in strict accordance with the Chinese Guideline for the Care and Use of Laboratory Animals (Ministry of Science and Technology [2006], File No. 398), and approved by the Animal Investigation Ethics Committee of the Affiliated Hospital of Qingdao University.

4.8. Statistical analysis

We conducted statistical analysis using GraphPad Prism 5 software. One-way analysis of variance (ANOVA) followed by Tukey's multiple-comparison test was applied to determine differences between groups. A value of $p < 0.05$ was considered to be statistically significant, and in the quantitative image, *, **, and *** corresponded to $p < 0.05$, $p < 0.01$, and $p < 0.001$, respectively. The results are expressed as the mean $\pm$ standard deviation (SD).

Data availability

The authors confirm that the data supporting the findings of this study are available within the article.

Author contributions

Peige Wang and Huajian Ren conceived and designed the experiments; Yangyang Liu, Shurui Song, Ruojing Li, Lei Song, and Yeying Zhao performed the experiments; Yangyang Liu and Zhiqiang Zheng analyzed the data; Peige Wang contributed reagents and materials; and Yangyang Liu and Yutong Liu wrote the manuscript.

Conflicts of interest

The authors declare no potential conflicts of interest with respect to the research, authorship, and/or publication with respect to this article.

Acknowledgements

References

1 Z. Yang, Z. C. Song, X. Nie, K. J. Guo and Y. Gu, *Stem Cell Res. Ther.*, 2020, **11**, 533.

2 X. Y. Yin, Y. P. Hao, Y. Lu, D. J. Zhang, Y. D. Zhao, L. Mei, K. Y. Sui, Q. H. Zhou and J. L. Hu, *Adv. Funct. Mater.*, 2021, **31**, 2105614.

3 W. C. Lineaweaver, *Ann. Plast. Surg.*, 2018, **81**, 1–2.

4 S. Kim, H. Y. Yoo, J. Huang, Y. Lee, S. Park, Y. Park, S. Jin, Y. M. Jung, H. B. Zeng, D. S. Hwang and Y. Jho, *ACS Nano*, 2017, **11**, 6764–6772.

5 Q. Saiding, Y. Y. Chen, J. Wang, C. L. Pereira, B. Sarmento, W. G. Cui and X. L. Chen, *Mater. Today Bio*, 2023, **21**, 100691.

6 S. Kalaba, E. Gerhard, J. S. Winder, E. M. Pauli, R. S. Haluck and J. Yang, *Bioact. Mater.*, 2016, **1**, 2–17.

7 W. J. Hu, S. L. Lu, Y. Ma, P. F. Ren, X. E. Ma, N. Z. Zhou, T. Z. Zhang and Z. L. Ji, *J. Mater. Chem. B*, 2017, **5**, 575–585.

8 J. Qiao, Z. W. Jiang, Y. Yang, J. H. Chi, X. S. Qiao, B. Q. Han and W. S. Liu, *Carbohydr. Polym.*, 2017, **172**, 255–264.

9 U. Fränneby, G. Sandblom, P. Nordin, O. Nyrén and U. Gunnarsson, *Ann. Surg.*, 2006, **244**, 212–219.

10 B. Calvo, G. Pascual, E. Peña, B. Pérez-Khöler, M. Rodríguez and J. M. Bellón, *J. Mech. Behav. Biomed. Mater.*, 2016, **59**, 366–378.

11 J. Skrobot, L. Zair, M. Ostrowski and M. El Fray, *Biomaterials*, 2016, **75**, 182–192.

12 I. S. Kikuchi, R. S. C. Galante, K. Dua, V. R. Malipeddi, R. Awasthi, D. D. Ghisleni and T. D. A. Pinto, *Curr. Drug Delivery*, 2017, **14**, 917–925.

13 Y. M. Kim, T. Potta, K. H. Park and S. C. Song, *Biomaterials*, 2017, **112**, 248–256.

14 X. Q. Zhou, Y. S. Li, S. Chen, Y. N. Fu, S. H. Wang, G. F. Li, L. Tao, Y. Wei, X. Wang and J. F. Liang, *Colloids Surf., B*, 2018, **172**, 601–607.

15 B. P. Lee, P. B. Messersmith, J. N. Israelachvili and J. H. Waite, *Annu. Rev. Mater. Res.*, 2011, **41**, 99–132.

16 H. Lee, N. F. Scherer and P. B. Messersmith, *Proc. Natl. Acad. Sci. U. S. A.*, 2006, **103**, 12999–13003.

17 B. Yang, N. Ayyadurai, H. Yun, Y. S. Choi, B. H. Hwang, J. Huang, Q. Y. Lu, H. B. Zeng and H. J. Cha, *Angew. Chem., Int. Ed.*, 2014, **53**, 13360–13364.

18 M. Mehdizadeh, H. Weng, D. Gyawali, L. P. Tang and J. Yang, *Biomaterials*, 2012, **33**, 7972–7983.

19 L. He, H. S. Liang, L. F. Lin, B. R. Shah, Y. Li, Y. J. Che and B. Li, *Colloids Surf., B*, 2015, **126**, 288–296.

20 C. Y. Chang, B. Duan, J. Cai and L. N. Zhang, *Eur. Polym. J.*, 2010, **46**, 92–100.

21 J. F. Shen, R. X. Chang, L. M. Chang, Y. Wang, K. L. Deng, D. Wang and J. L. Qin, *Carbohydr. Polym.*, 2022, **281**, 119052.

22 S. Bang, Y. G. Ko, W. I. Kim, D. Cho, W. H. Park and O. H. Kwon, *Int. J. Biol. Macromol.*, 2017, **105**, 886–893.

23 K. G. Satyanarayana, G. G. C. Arizaga and F. Wypych, *Prog. Polym. Sci.*, 2009, **34**, 982–1021.

24 K. Moffatt, Y. J. Wang, T. R. R. Singh and R. F. Donnelly, *Curr. Opin. Pharmacol.*, 2017, **36**, 14–21.

25 E. Larrañeta, R. E. M. Lutton, A. D. Woolfson and R. F. Donnelly, *Mater. Sci. Eng., R*, 2016, **104**, 1–32.

26 H. Y. Mi, M. R. Salick, X. Jing, B. R. Jacques, W. C. Crone, X. F. Peng and L. S. Turng, *Mater. Sci. Eng. C*, 2013, **33**, 4767–4776.

27 Y. J. Zhong, J. Wang, Z. Y. Yuan, Y. Wang, Z. H. Xi, L. Li, Z. Y. Liu and X. H. Guo, *Colloids Surf., B*, 2019, **179**, 462–469.

28 I. C. Lee, J. S. He, M. T. Tsai and K. C. Lin, *J. Mater. Chem. B*, 2015, **3**, 276–285.

29 S. Van Hoef, P. Dries, M. Allaeys, H. H. Eker and F. Berrevoet, *Hernia*, 2024, **28**, 701–709.

30 C. R. Xiao, L. Fan, S. Q. Zhou, X. C. Kang, P. F. Guan, R. M. Fu, C. H. Li, J. Ren, Z. A. Wang, P. Yu, Y. Wang, C. L. Deng, L. Zhou and C. Y. Ning, *ACS Nano*, 2022, **16**, 20770–20785.

31 X. Peng, X. F. Xia, X. Y. Xu, X. F. Yang, B. G. Yang, P. C. Zhao, W. H. Yuan, P. W. Y. Chiu and L. M. Bian, *Sci. Adv.*, 2021, **7**, eabe8739.

32 Q. Zou, C. Liu, N. Hu, W. Wang and H. Wang, *Mol. Biol. Rep.*, 2022, **49**, 2985–2998.